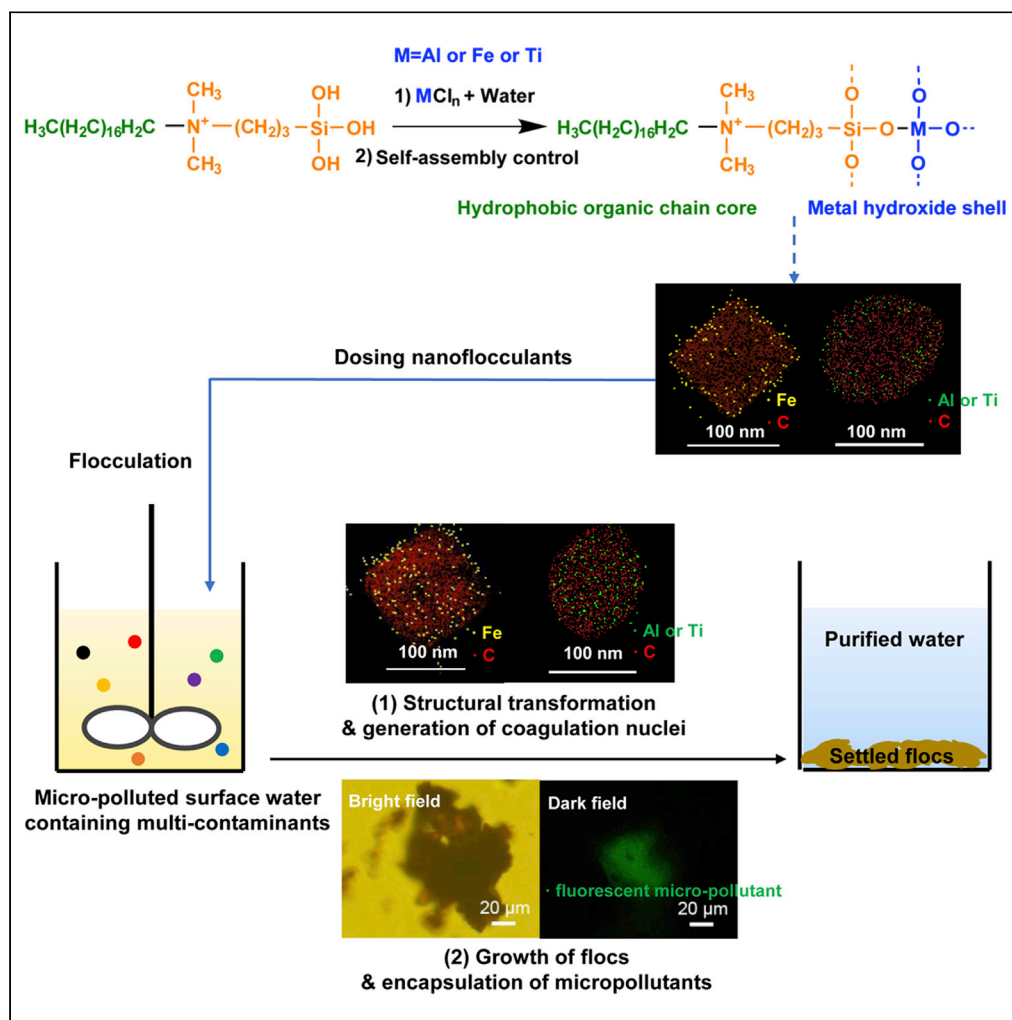# iScience

Article

Hydrophobic-modified metal-hydroxide nanoflocculants enable one-step removal of multi-contaminants for drinking water production

Zhen Yang, Lina Zhao, Min Hu, ..., Peiyong Qin, Weiben Yang, Nigel J.D. Graham

yangzhen@njnu.edu.cn

Highlights

Hydrophobic-organic-chain-modified metal hydroxide (HOC-M) flocculants are designed.

HOC-M removes various contaminants in a single step from river water.

HOC-M produced flocs with better structural and dewatering properties.

Nano-structure transformation promotes formation of meso-scale coagulation nuclei.

iScience

Article

Hydrophobic-modified metal-hydroxide nanoflocculants enable one-step removal of multi-contaminants for drinking water production

Zhen Yang,[1,6,*] Lina Zhao,[1] Min Hu,[1] Di Cai,[3] Ziqi Tian,[4] Jan Baeyens,[3,5] Raf Dewil,[5] Peiyong Qin,[3] Weiben Yang,[1] and Nigel J.D. Graham[2]

SUMMARY

Flocculation is a mainstream technology for the provision of safe drinking water but is limited due to the ineffectiveness of conventional flocculants in removing trace low-molecular-weight emerging contaminants. We described a synthesis strategy for the development of high-performance nanoflocculants (hydrophobic-organic-chain-modified metal hydroxides [HOC-M]), imitating surfactant-assembling nano-micelles, by integration of long hydrophobic chains with traditional inorganic metal (Fe/Al/Ti)-based flocculants. The core-shell nanostructure was highly stable in acidic stock solution and transformed to meso-scale coagulation nuclei in real surface water. In both jar and continuous-flow tests, HOC-M was superior over conventional flocculants in removing many contaminants (turbidity, UV_{254}, and DOC: >95%; TP and NO_3-N: >90%; trace pharmaceuticals [initial concentration: 100 ng/L]: >80%), producing flocs with better structural and dewatering properties, and lowering the environmental risk of metal leaching. The rationally designed nanoflocculants have large application potential, as a solution to increasing public concern about micro-pollutants and increasing water quality requirements.

INTRODUCTION

The provision of safe drinking water is one of the top priorities for humanity, according to the UN's 2030 Sustainable Development Goal 6 (Larsen et al., 2016; United Nations, 2021; https://sdgs.un.org/goals/goal6). However, the worsening contamination of surface waters for drinking water supplies remains a worldwide challenge (Miller et al., 2017). In addition to commonly present water pollutants (suspended solids [SS], natural organic matter [NOM], inorganic nutrients, etc.), as represented by conventional water quality parameters (turbidity, UV_{254}, dissolved organic carbon [DOC], total phosphates [TP] and NO_3^--N, etc.), emerging micro-pollutants, such as anthropogenic pharmaceuticals, are frequently detected in surface water and are of growing concern (Benner et al., 2013; Grandclement et al., 2017). These micro-pollutants, although present at trace level (ng/L—μg/L), are associated with risks of chronic negative effects on human health through continuous exposure and bioaccumulation. They are difficult to remove by conventional drinking water treatment techniques (like flocculation-sedimentation-sand filtration) in established water treatment works (WTWs), because conventional methods are unable to aggregate small-sized low-molecular-weight organic contaminants at ultra-low concentrations to meso-scale coagulation nuclei for separation by sedimentation (Richardson and Kimura, 2020; Schwarzenbach et al., 2006).

In the past decades, much research has been focused on additional treatment methods, including adsorption, membrane separation, and advanced oxidation processes (AOPs), for the effective removal of emerging micro-pollutants (Alsbaiee et al., 2016; Chen et al., 2019; Miller et al., 2017). Despite their achievements, most of the previous studies have relied on the performance (e.g., greater removal of SS and NOM) of conventional pretreatment methods, thereby creating more complex water treatment processes with a higher cost and land occupation (Benner et al., 2013; Decrey et al., 2020; Grandclement et al., 2017). Alternative approaches that are capable of reducing the concentration of a wide range of micro-pollutants in surface raw waters by using simpler and more efficient processes would be advantageous (Shannon et al., 2008). Thus the development of novel methods of improving existing processes in

[1]School of Chemistry and Materials Science, Jiangsu Provincial Key Laboratory of Material Cycling and Pollution Control, Nanjing Normal University, Nanjing 210046, China

[2]Department of Civil and Environmental Engineering, Imperial College London, London, SW7 2AZ, UK

[3]College of Life Science and Technology, National Energy R&D Center for Biorefinery, Beijing University of Chemical Technology, Beijing 100029, China

[4]Ningbo Institute of Materials Technology & Engineering, Chinese Academy of Sciences, Ningbo 315000, China

[5]Department of Chemical Engineering, Process and Environmental Technology Lab, KU Leuven, 2860 Sint-Katelijne-Waver, Belgium

[6]Lead contact

*Correspondence: yangzhen@njnu.edu.cn

https://doi.org/10.1016/j.isci.2021.102491

established WTWs offers greater cost-effectiveness and will be of value to both end users and policy-makers in the water supply industry (Herrmann et al., 2017).

Flocculation is a cost-effective and easy-to-operate water treatment technology with a long history and remains a mainstream process in WTWs (Ding et al., 2018; Wang et al., 2018; Yu et al., 2019). During the process, flocculants, through multi-effects, promote the aggregation (coagulation) of colloidal contaminants (such as SS and NOM) and the growth of amorphous, solid-phase flocs (Yu et al., 2019), which are subsequently separated from water by sedimentation/flotation. However, an obstacle limiting the application of conventional flocculants (e.g., inorganic metal hydroxides) in micro-polluted water treatment is their ineffectiveness in the removal of trace dissolved contaminants with low molecular weight, including pharmaceuticals with high environmental risks in water, as aforementioned (Grandclement et al., 2017; Liu et al., 2019; Wang et al., 2020b). The decoration of hydrophobic functional groups onto hydrophilic natural polymers has been proved to be feasible for enhancing the ability of both the formation of solid-phase coagulation nuclei and the binding between flocculants and emerging small-molecular-weight micro-pollutants (Ren et al., 2017; Yang et al., 2016, 2020). Nevertheless, a simple combination of hydrophobic groups with conventional flocculants could negate the flocculants' dispersibility in stock solution, leading to reduced available interaction sites of dosed flocculants toward the contaminants (Du et al., 2018).

Nanotechnology has demonstrated considerable potential in various water remediation methods, especially in AOPs, adsorption, and membrane filtration (Chen et al., 2019; Gu et al., 2019; Wang et al., 2016; Zhang et al., 2019a, 2019b). However, studies employing nanotechnology in flocculation are relatively few (Simate et al., 2012; Yang et al., 2013). It is known that nano-sized micelles, with a core-shell structure (a core of hydrophobic chains and a shell of polar groups) in water, self-assembled by surfactants under suitable conditions, have extra stability and dispersibility in the solvent (Hamley 2003; Holmberg et al., 2002; Jiang et al., 2006). Micelles can encapsulate hydrophobic small-molecular contaminants in the core, whereas their surfaces are able to interact flexibly with other hydrophilic contaminants (Qin et al., 2019; Sun et al., 2014). Inspired by the nature of the nano-sized micelles, we report here a simple and versatile approach to synthesize "micelle-like" nanoflocculants by integration of long hydrophobic organic chains (octadecyl groups) with hydrophilic metal (Fe/Al/Ti) hydroxides, bridged by (trimethoxysiloxy)propyldimethylammonium (Figure 1A). In addition to the desired dispersibility (Supplemental information Figure S1) in acidic stock solutions, the hydrophobic-organic-chain-modified metal hydroxides (HOC-M) combine the flocculation ability of traditional metal salt/hydroxide flocculants (for colloidal contaminants) with that of hydrophobic groups for emerging micro-pollutants and are able to efficiently remove a wide range of contaminants from micro-polluted surface water in a single treatment step.

RESULTS AND DISCUSSION

Characteristics of the nanoflocculants

Chemical structures of the as-prepared nanoflocculants were identified by characteristic peaks in Fourier transform infrared spectra (Figures 1B and S2). For HOC-M formed by the same metal element but with different molar ratios of octadecyl: metal atoms (O/M ratios of 1:5, 1:10, and 1:15) in the raw materials, the intensities of Si-O-M bonds first increased with O/M ratio rising from 1:5 to 1:10, due to the increasing degree of cross-linking of siloxy groups by the metal oxide/hydroxide shells (Figure S2); however, when excessive metal salts were added for the synthesis, metal oxides/hydroxides are preferentially self-bridged in the outer layer, engendering decreased Si-O-M intensities.

Micro-morphologies of HOC-M were observed using transmission electron microscopy (TEM) (Figures 1C–1E and S3). The corresponding particle size distribution was inserted in each figure. All HOC-M are mono-dispersed nanoparticles. Among them, the HOC-Fe series is cubic with round corners, whereas the HOC-Al and HOC-Ti series are spherical. Average diameters of different samples (Figure 1F) showed that the sizes of the nanoparticles with the same metal atoms underwent a "down-bottom-up" trend as the metal contents increased. Such a pattern is consistent with the above-mentioned intensity changes of Si-O-M bonds: before reaching the optimal dosage, increasing amounts of "cross-linking agent" metal oxide/hydroxide enhanced the restriction of inner chains of the nanoparticles, causing the decreased size; however, excessively dosed metal ions form self-bridged metal oxides/hydroxides outside, leading to thicker shell layers. The size of different HOC-M series with different metal atoms followed the order of
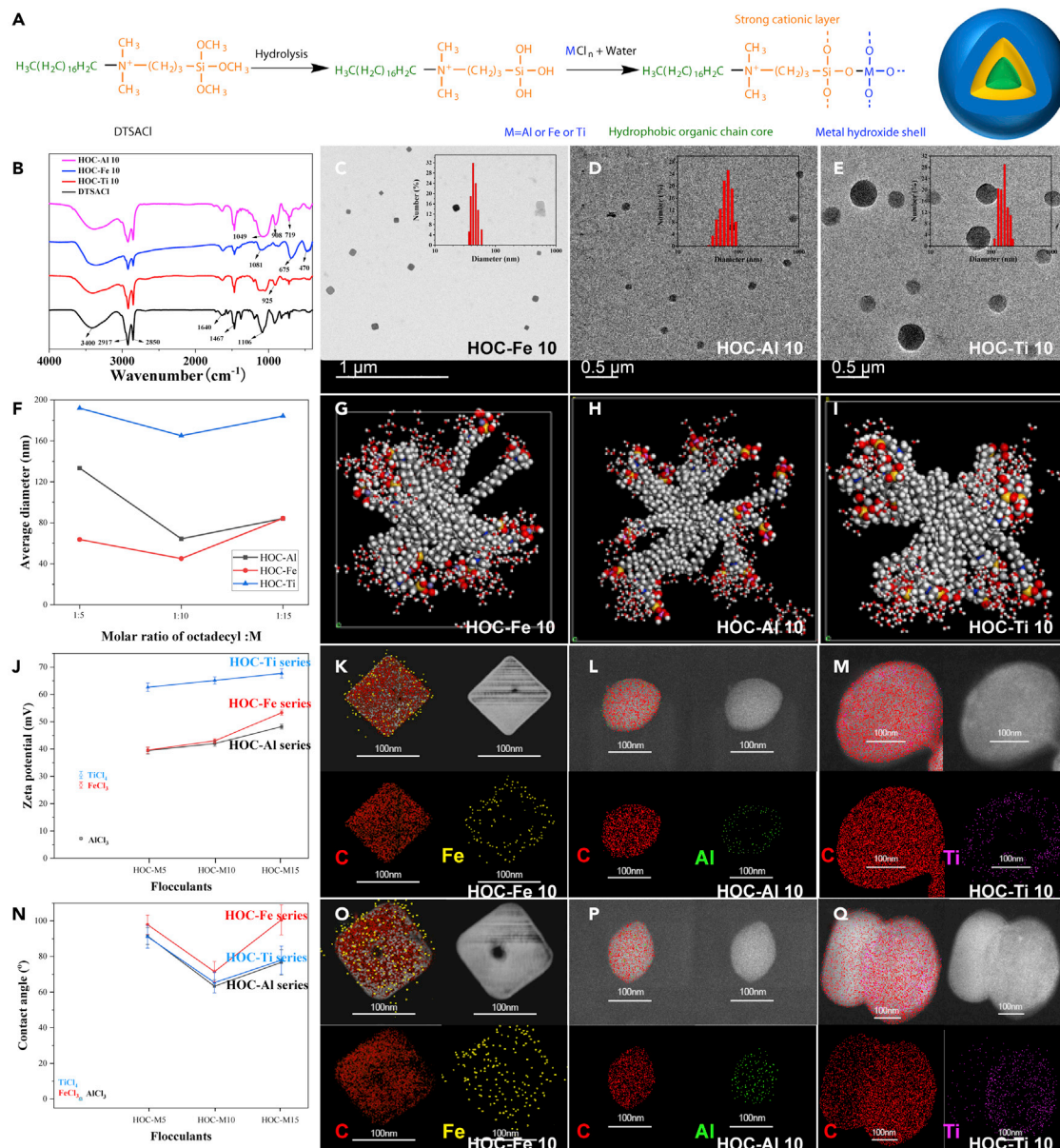
Figure 1. Synthetic route and characterizations of HOC-M

(A) Synthetic route of HOC-M.

(B) Fourier transform infrared spectra of the raw material and HOC-M.

(C–E) TEM images of HOC-M (inset: size distribution measured by light scattering).

(F) Changes of number-average diameters as functions of molar ratios of octadecyl:M in HOC-M (calculated from the size distribution curves in the inset figures of Figures 1C–1E).

(G–I) MD computation results of HOC-M.

(J) ZPs of traditional metal salt flocculants and HOC-M (calculated from triplicated parallel tests [n = 3]).

(K–M) TEM-EDX elemental mapping of HOC-M in stock solution (total metal concentration: 0.1 mol/L).

(N) WCAs of quartz slices coated with metal salts and HOC (calculated from triplicated parallel tests [n = 3]).

(O–Q) TEM-EDX elemental mapping of HOC-M after added into water with a pH of ~7.44 for flocculation for 20 s (HOC-M dosage: 120 mg/L).

HOC-Fe < HOC-Al < HOC-Ti, which was consistent with the order of M-O bond energy (Fe-O: 409 kJ/mol; Al-O: 512 kJ/mol; Ti-O: 662 kJ/mol) (Dean and Lange, 1999). A stronger M-O bond implied a stronger potential for metal oxides/hydroxides formation in the shell layers, which produced larger HOC-M particles.

The core-shell structures of the nanoflocculants were demonstrated by molecular dynamic (MD) computations (Figures 1G and 1I), zeta potential (ZP) determination (Figure 1J), and TEM-energy dispersive X-ray (EDX) mapping (Figures 1K–1M). In Figures 1G–1I, hydrophobic organic chains assembled inside through hydrophobic association, whereas metal oxides/hydroxides faced outward as shells. Compared with corresponding conventional flocculants (inorganic metal salts), the HOC-M particles had notably greater ZPs (Figure 1J), due to the contribution of both the outward metal oxides/hydroxides and the ammonium groups. For each HOC-M series, the ZPs of HOC-M increased with the accumulation of metal atoms in the shells. The increasingly positive ZPs of the nanoflocculants were beneficial for improving not only the stability of nanoparticles in the stock solution but also the capacity for removing negatively charged water contaminants in flocculation (Wang et al., 2020a). TEM-EDX images visualized the micro-structures of HOC-M in stock solutions (Figures 1K–1M), where C filled the core and metal elements were only distributed in the exterior.

The core-shell configuration of HOC-M in stock solutions could be transformed under certain conditions. Water contact angles (WCAs) of quartz slices coated with metal salts remained zero; however, after coating with HOC-M, quartz slices had notably larger WCAs (Figure 1N and Figure S4), indicating that the core-shell configuration of HOC-M experienced a transformation process, during which the metal oxide/hydroxide shell bound with the quartz surface and the hydrophobic chains exposed outside. Two factors affected the aforementioned transformation process: the cross-linking strength of the metal oxide/hydroxide shell and the binding strength between the shell and the quartz surface. For HOC-M 5, inadequate cross-linking strength of the shell (due to insufficient metal oxide/hydroxide) led to more flexible hydrophobic chains with less restriction in the core, which engendered more facile transformation of the core-shell structure; for HOC-M 10, the increased cross-linking strength of the shell inhibits the transformation; for HOC-M 15, despite the further increased cross-linking strength, binding (electrostatic attraction and H-bonding) between the quartz surface and the large amounts of metal oxide/hydroxide became very strong, which promoted the transformation process again. Therefore, for the same metal atom, HOC-M 10 had the lowest WCA in Figure S4, whereas HOC-M 5 (M = Al or Ti) or HOC-M 15 (M = Fe) had the largest value. The transformation of the core-shell configuration could also be detected after HOC-M was added into water with a pH of ∼7.44 (similar pH to the Yangtze River water sample used in this work) for a flocculation time of 20 s; the original metal-hydroxide shell structure was destroyed with metal elements uniformly distributed in the nanoparticles (Figures 1O–1Q). Moreover, the structural transformation and shell hydrolysis were found to contribute to the generation of primary meso-scale coagulation nuclei and the formation of subsequent flocs, as particle size continued to increase after HOC-M was added into water (pH = ∼7.44) (Figure S5).

N-containing disinfection by-product (N-DBP) detection and acute toxicity assays of the nanoflocculants were also tested, considering possible environmental concerns of the quaternary ammonium groups and the nanostructure of HOC-M. With nine typical N-DBPs (involving N-nitrosodimethylamine [NDMA], N-nitrosodiethylamine [NDEA], N-nitrosomethylethylamine [NEMA], N-nitrosopyrrolidine [NPYR], N-nitrosomorpholine [NMOR], N-nitrosodi-n-propylamine [NDPA], N-nitrosopiperidine [NPIP], N-nitrosodi-n-butylamine [NDBA], and N-nitrosodiphenylamine [NDPhA]) used as reference (Table S1), no detectable N-DBP was found in the chloramine-treated flocculant solution (HOC-M10 concentration of 10 mg/L; Figure S6). Toxicity test results (Figure S7) showed that HOC-Al10, HOC-Fe10, and HOC-Ti10 had 24-h half maximal effective concentration (24h-EC50) of 24.63, 80.04, and 36.11 mg/L, respectively, which were two or three log-units larger than the value of traditional inorganic flocculant polyaluminum chloride (PACl), as reported (Yang et al., 2014b). The results demonstrated the much lower acute toxicity of the newly prepared nanoflocculants.

Water treatment performance

The flocculation performance of HOC-M was assessed using both a static jar flocculator (Figure 2A; the most widely applied in laboratories) and a continuous-flow apparatus (Figures 2B and 2C; a simplified and reduced-scale model of real facilities in WTWs). Samples of raw surface water (water quality parameters listed in Table S2) were collected from the Ma'anshan section of Yangtze River (31°38′49″N 118°27′06″E).

In jar tests, based on values of removal efficiency (RE)—dosage profiles of each HOC-M series (Figures S8–S10), HOC-M10 with an O/M ratio of 1:10 always showed a better performance (lower optimal dosage and/or higher maximum RE) than HOC-M5 and HOC-M15. Such an O/M ratio-dependent performance could be
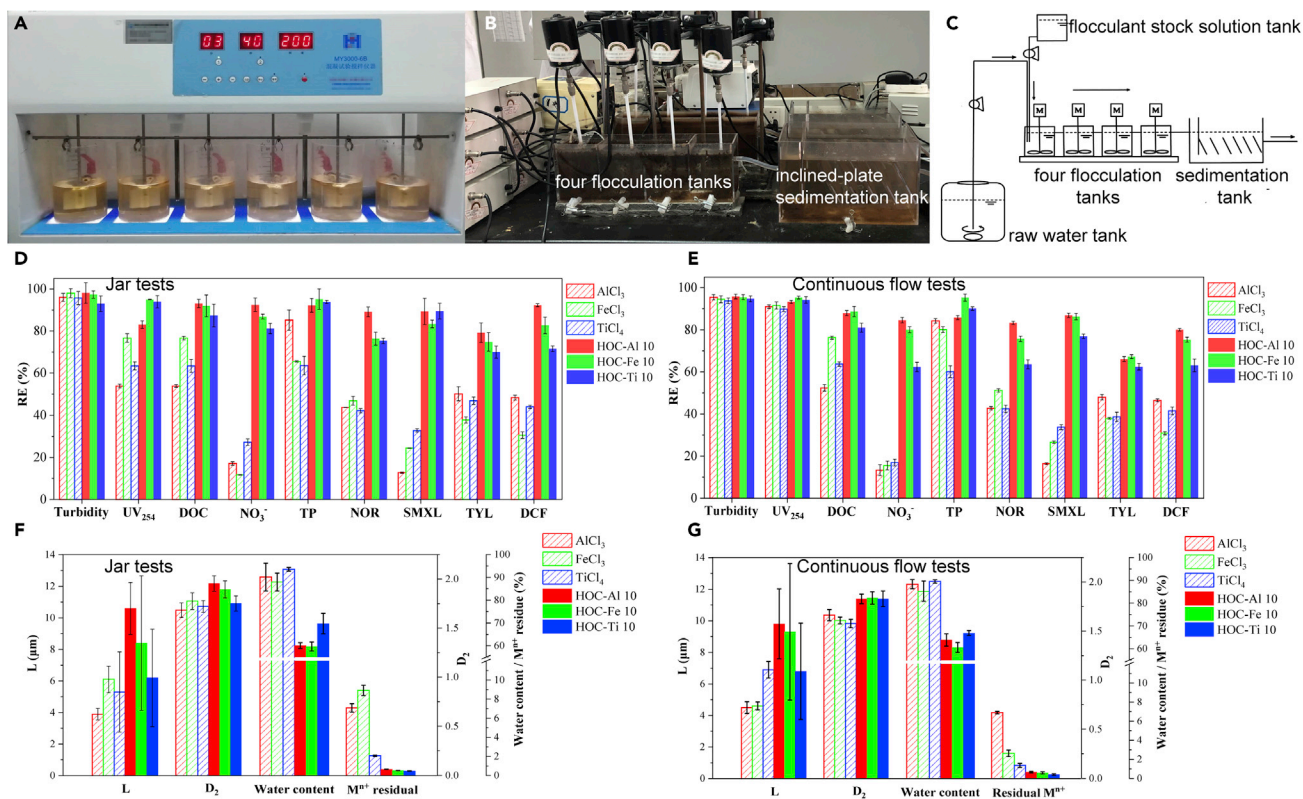
Figure 2. Experimental setups and results for water treatment tests

(A) Photograph of the experimental setup for jar flocculation tests.

(B and C) (B) Photograph and (C) schematic representation of the experimental setup for continuous-flow flocculation tests.

(D and E) Maximum REs of various contaminants from Yangtze River water at corresponding optimal dosages of various flocculants in (D) jar and (E) continuous-flow tests, (every RE was calculated from triplicated parallel tests [n = 3]).

(F and G) Sizes (L), two-dimensional fractal dimensions (D_2), and dewatering properties of flocs, as well as metal leaching rates, at corresponding optimal dosages of various flocculants in (F) jar and (G) continuous-flow tests, respectively (each data point was calculated from triplicated parallel tests [n = 3]).

related to the changes of size (Figure 1F) and WCA (Figure 1N), implying that the O/M ratio should be well-controlled for the optimum HOC-M nanoflocculant. In contrast, the O/M ratio-dependent performance was not related to ZP change (Figure 1J); the optimum HOC-M10 had neither the highest nor the lowest ZP. This result demonstrated that charge attraction played a role, but was not the only influencing factor in the flocculation.

The REs of conventional flocculants (FeCl₃, AlCl₃, and TiCl₄) in both jar and continuous-flow tests (Figure S11 and S12), as well as those of HOC-M10 in continuous-flow tests (Figure S13), were also determined for comparison. In this case, each of the model pharmaceutical contaminants (norfloxacin [NOR], sulfamethoxazole [SMXL], tylosin [TYL], and diclofenac [DCF]) with various characteristics and molecular species distribution (Table S3 and Figure S14) was frequently detected in real waters (Benner et al., 2013) and was manually added into the surface water samples to reach an initial equilibrium concentration of 100 ng/L (within the commonly detected concentration range in real micro-polluted water) for treatment (Richardson and Kimura, 2020; Schwarzenbach et al., 2006); such a trace concentration of pharmaceuticals is known to be difficult to remove (Grandclement et al., 2017; Shannon et al., 2008). The summarized results of both jar and continuous-flow tests in Figures 2D and 2E had similar conditions. All flocculants could efficiently remove turbidity (>95%) as the turbidity-causing suspended colloids in surface water are typically easy to flocculate. For other parameters, metal salts exhibited a range of REs as follows: UV₂₅₄ (50%–90%), DOC (50%–80%), NO₃-N (10%–30%), TP (60%–90%), and pharmaceuticals (10%–50%). The relatively poor performance of metal salt flocculants in removing dissolved small-sized molecules was consistent with that reported in previous studies (Decrey et al., 2020; Ren et al., 2017; Richardson and Kimura, 2020).
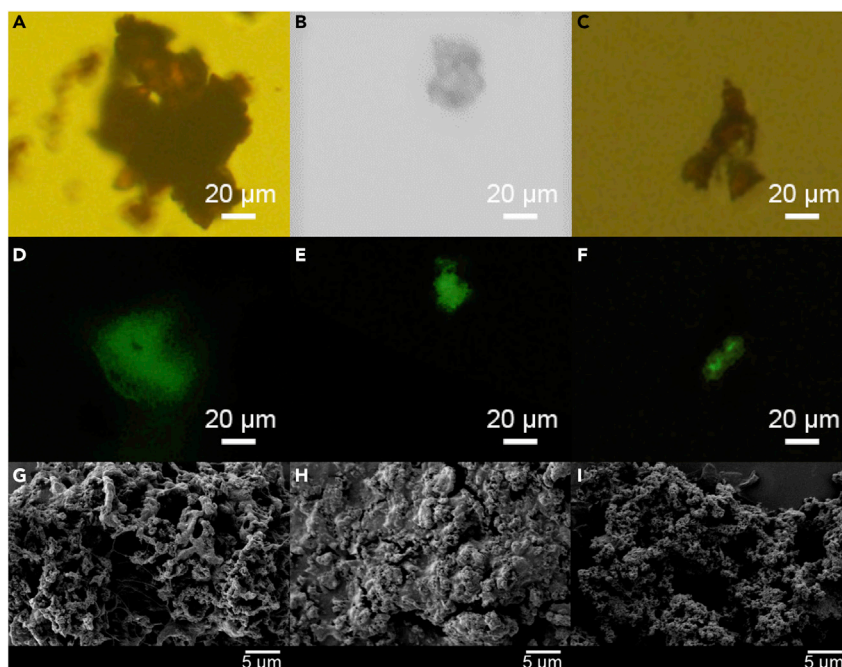
Figure 3. Morphological characteristics of flocs formed at corresponding optimal flocculant dosages in jar tests

(A–F) (A–C) Bright-field and (D–F) dark-field images of flocs formed by flocculation of 3,3'-diethylthiacyanine iodide (10 mg/L)-added Yangtze River water at corresponding optimal dosages of various flocculants in jar tests (A and D: HOC-Al10; B and E: HOC-Fe10; C and F: HOC-Ti10).

(G–I) SEM images of freeze-dried flocs at corresponding optimal dosages of various flocculants in jar tests (G: HOC-Al10; H: HOC-Fe10; I: HOC-Ti10).

In contrast to metal salts, the HOC-M10 nanoflocculants displayed improved REs for all water quality parameters, including both the conventional parameters and the four pharmaceutical compounds (Figures 2D and 2E). In addition, compared with the already reported hydrophobic modified chitosan flocculant, which could remove ~80% of NOR and ~70% of TYL in flocculation-sedimentation process (Yang et al., 2020), HOC-Al10 demonstrated better REs for those trace pharmaceuticals. The notable improvement of HOC-M10 in the removal of trace organic contaminants was exhibited visually by fluorescence microscopic observation. A fluorescent molecular probe, 3,3'-diethylthiacyanine iodide, was employed to represent the small-molecular contaminants. Flocs containing 3,3'-diethylthiacyanine iodide formed by all flocculants in jar tests were found in bright fields (Figures 3A–3C and S15A–S15C), demonstrating that HOC-M10, as well as commercial flocculants, had the ability to destabilize and aggregate large-sized contaminants. However, in dark fields (Figures 3D–3F and S15D–S15F), fluorescent aggregates could only be found for HOC-M10, but not for metal salts. This phenomenon suggested that the metal salt flocculants could hardly aggregate the small-sized organic molecules into flocs, whereas these organic contaminants in solution were encapsulated into HOC-M10-induced solid flocs. Among the three HOC-M10 flocculants, it was HOC-Al10 or HOC-Fe10 (but never HOC-Ti10) that had the maximum RE (RE_{max}) for a certain contaminant (Figures 2D and 2E). For the different pharmaceuticals, the RE_{max} of TYL was smaller than any RE_{max} of the other three pharmaceuticals. As the main species of TYL in the test water was cationic (Figure S14D) and TYL had the largest molecular weight (Table S3) among the four pharmaceuticals, it would be the most difficult for TYL to be encapsulated into the interior of the flocs.

In addition to the removal of various contaminants, a comprehensive evaluation of the performance of the flocculants included the corresponding floc/sludge properties (sizes [L] and two-dimensional fractal dimensions [D_2] of flocs, water contents of mechanically compressed sludge, and specific filtration resistance [SFR] and capillary suction time [CST] of settled sludge) and residual metal ions in treated water (Figures 2F, 2G, and S16–S18), which are also of great significance for industrial applications (Chakraborti et al., 2000; Wang et al., 2018; Wu et al., 2020). Compared with metal salts, HOC-Al10 or HOC-Fe10 produced flocs with larger L and larger D_2 (representing more compact flocs) (Figures 2F and 2G); these flocs were

easier to settle and can shorten the water treatment time (Chakraborti et al., 2000). Compared with flocs generated by the already reported hydrophobic modified chitosan flocculant (with an L of 21.38 μm and a D_2 of 1.65) (Yang et al., 2020), those formed by HOC-M10 were more compact (with larger D_2), but smaller in size; this was attributed to the fact that the chitosan-based organic flocculant had a much larger molecular weight and longer polymer chains, which exerted a strong bridging flocculation effect and led to larger flocs. According to the SFRs and CSTs of sludge formed in continuous flow tests (Figure S18), sludge produced by HOC-M10 (especially HOC-Al10) had smaller SFR and CST, implying a better dewatering property (higher water permeability) of those flocs with reduced energy costs in the further dewatering process. After mechanical compression, the HOC-M10-generated flocs had much lower water contents (60%–70%) than metal-salt-generated ones (~90%); such an advantage of HOC-M10 would reduce subsequent disposal costs of the compressed sludge (Wu et al., 2020). The improved dewatering performance was ascribed to the weakened H-bonding between water and HOC-M10 with additional hydrophobic chains (Wu et al., 2020). Scanning electron microscopic images of flocs after freeze-drying (Figures 3G–3I and S19) showed that, compared with metal salts, HOC-M10 generated sponge-like flocs with remarkably larger pores and cracks, which assisted water to be released during floc compression.

Metal ion leaching rates in the treated water by the self-assembled nanoflocculants were an order of magnitude lower than those of traditional soluble metal salts (Figures 2F and 2G). As the chemical bonds between long organic chains and metal hydroxide are difficult to break under mild flocculation conditions at room temperature, the residual metal contents in the effluent here could be an indicator that partially represents the remaining flocculant in the treated water. The metal leaching rates of HOC-M (lower than 1% of the dosage) indicated the low concentration (<1.2 mg/L) of remaining HOC-M. As aforementioned, no N-DBP was detected in the chloramine-treated flocculant solution for 10 mg/L HOC-M. Therefore, N-DBP formation is unlikely to be significant in the treated water during possible subsequent disinfection. Furthermore, considering the above-mentioned low acute toxicity of HOC-M with 24hr-EC50 larger than 20 mg/L, it is likely that the application of HOC-M10 can reduce the environmental and health risks caused by residual flocculants in water (Wang et al., 2018).

Mechanism investigation

All the results above-described displayed a notable superiority of HOC-M (especially HOC-Fe10 and HOC-Al10) flocculants over conventional metal salts in the treatment of micro-polluted surface water. The fundamental mechanisms responsible for the performance enhancement were investigated and are discussed as follows. After dosing the flocculants to the surface water samples, the ZP of colloids in the solution increased (more positive) with increasing dosage (Figure 4A). The upward trends verified the existence of charge attraction between the flocculants and contaminants, which arose from two cationic parts of the nanoflocculants—the metal hydroxide in the shell (Figures 1K–1M) and the quaternary ammonium groups. The contribution of the latter was detected by X-ray photoelectron spectra (XPS; Figures 4B, 4C, and S20). These showed new NO_3^--N and amino-N peaks in flocs due to the incorporation of NO_3^- and NOM; the blue shift of the NR_4^+-N peak from 401.26 eV in HOC-M10 to ~402.30 eV in the flocs indicated the occurrence of charge attraction at the quaternary ammonium sites. However, charge attraction was not the only effect driving flocculation, as the ZP should be approximately zero at the optimal dosage if charge attraction predominated (Yang et al., 2014a). Thus the phenomenon of ZPs much larger than zero within the optimal dosage range (Figure 4A) indicated that other factors were involved.

Binding interactions between the nanoflocculants and the main species of dissolved contaminants in water were examined using density functional theory (DFT) computations (Figures 4D–4J, S21, and S22). Considering the optimized geometries of HOC-Al10 system as illustrations (Figures 4D–4J), different contaminants were inclined to be bound by different sites of the flocculant. (1) For the outer layer part of the nanoflocculant, humic acid (HA, a model substance representing NOM), NO_3^-, and HPO_4^{2-} were bound and removed (Figures 4D–4F). Among them, NO_3^- was mainly bound by the quaternary ammonium sites, whereas HPO_4^{2-} was strongly coordinated with a large binding energy (BE) by metal atoms. HA, with a relatively larger molecular structure, was bound to both metal atoms (via coordination with oxygen-containing groups) and quaternary ammonium groups (via electrostatic attraction with the quaternary ammonium sites). (2) For the inner part (the long organic chain) of HOC-M, trace pharmaceuticals were captured and eliminated (Figures 4G–4J). This finding agreed with the aforementioned encapsulation effect observed in fluorescence microscopic images (Figures 3D–3F). In addition to charge attraction between the negatively charged groups of the pharmaceuticals (except for TYL, which was mainly cationic at
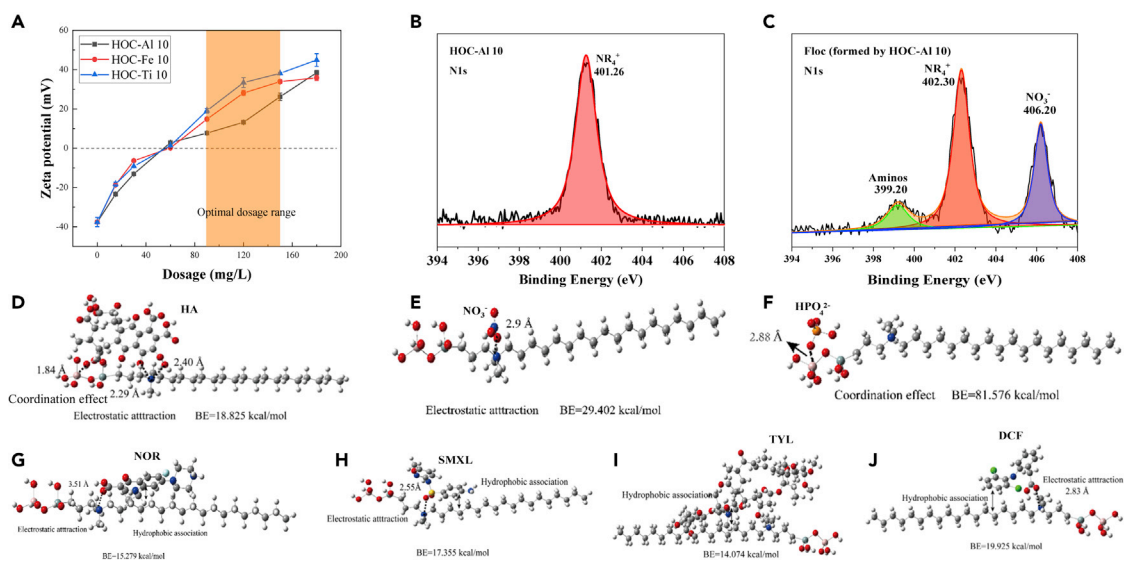
Figure 4. Mechanistic investigation results on interfacial interactions between flocculants and contaminants

(A) ZP dosage profiles of Yangtze River water after the dose of HOC-M10 (each data point was calculated from triplicated parallel tests [n = 3]).

(B and C) XPS spectra of (B) HOC-Al10 and (C) flocs formed by HOC-Al10 at its optimal dosage.

(D–J) DFT calculation results (optimized configurations and corresponding binding energies [BEs]) of different complexes of flocculant (HOC-Al10)-contaminant.

pH = 7.44) and HOC-M's quaternary ammonium, the hydrocarbyls of these contaminants were tightly bound through hydrophobic association by hydrophobic long chains of the nanoflocculant (Figures 4G–4J). Among all four pharmaceutical compounds, TYL had the smallest BE, which was consistent with the relatively lower RE(TYL) than the RE of the other three pharmaceuticals, as discussed above and shown in Figures 2D and 2E.

Although a limited number of model pollutants were tested in this work, guidance on the removal of other types of pollutants could be suggested according to the aforementioned results, as follows: pharmaceuticals with similar chemical structures may be efficiently removed; contaminants in anionic species, compared with those in cationic species, at near-neutral pH may be easier to remove, due to the existence of positively charged groups in HOC-M; and organic pharmaceutical molecules with hydrocarbyls may be more easily captured by the long organic chains of HOC-M and then eliminated.

Challenge and prospects

The aforementioned results have demonstrated the significantly improved performance of the nanocomposite flocculants HOC-M. For further development of HOC-M toward practical applications, one challenge remains with respect to the costs. As a preliminary evaluation, unit prices of HOC-M10 were calculated and summarized in the Table S4, according to the current laboratory-scale preparation method and the market prices of different raw materials. Compared with the unit prices of traditional flocculants, those of HOC-M10 were higher. Thus, an investigation of an alternative low-cost synthesis process would be of value in future work. On the other hand, regeneration and reuse of flocculants from flocs might be another solution (Ren et al., 2017). Furthermore, as HOC-M was efficient in the removal of a wide range of contaminants in the flocculation process, the difficulty and complexity of subsequent processes in the combined water treatment technologies may be decreased substantially, accompanied by a potential cost reduction of the entire treatment process.

Limitations of the study

As aforementioned, although HOC-M10 showed superior performance than conventional flocculants, their unit prices were much higher, which could be a notable factor limiting their application in real water treatment. How to reduce the production cost by optimizing the synthesis process still needs further study. In addition, for the reuse of the flocculants, which is another aspect for the control of water treatment cost, investigation and development of the flocculant regeneration process is also needed.

STAR★METHODS

Detailed methods are provided in the online version of this paper and include the following:

- KEY RESOURCES TABLE
- RESOURCE AVAILABILITY
  - Lead contact
  - Materials availability
  - Data and code availability
- EXPERIMENTAL MODEL AND SUBJECT DETAILS
- METHOD DETAILS
  - Synthesis of HOC-M
  - Flocculation tests
  - Characterizations and analyses
  - Theoretical chemical computations
- QUANTIFICATION AND STATISTICAL ANALYSIS

SUPPLEMENTAL INFORMATION

Supplemental information can be found online at https://doi.org/10.1016/j.isci.2021.102491.

AUTHOR CONTRIBUTIONS

Conceptualization, Z.Y. and L.Z.; methodology, Z.Y., L.Z., M.H., and W.Y.; software, L.Z. and Z.T.; investigation, Z.Y. and L.Z.; writing – original draft, Z.Y.; writing – review & editing, Z.Y., M.H., D.C., J.B., R.D., P.Q., and N.J.D.G.; supervision, Z.Y.; funding acquisition, Z.Y. and W.Y.

DECLARATION OF INTERESTS

The authors declare no competing interests.

REFERENCES

Alsbaiee, A., Smith, B.J., Xiao, L.L., Ling, Y.H., Helbling, D.E., and Dichtel, W.R. (2016). Rapid removal of organic micropollutants from water by a porous beta-cyclodextrin polymer. Nature *529*, 190–194.

Benner, J., Helbling, D.E., Kohler, H.P.E., Wittebol, J., Kaiser, E., Prasse, C., Ternes, T.A., Albers, C.N., Aamand, J., Horemans, B., et al. (2013). Is biological treatment a viable alternative for micropollutant removal in drinking water treatment processes? Water Res. *47*, 5955–5976.

Chakraborti, R.K., Atkinson, J.F., and Van Benschoten, J.E. (2000). Characterization of alum floc by image analysis. Environ. Sci. Technol. *34*, 3969–3976.

Chen, Y., Zhang, G., Liu, H., and Qu, J. (2019). Confining free radicals in close vicinity to

contaminants enables ultrafast fenton-like processes in the interspacing of MoS2 membranes. Angew. Chem. Int. Ed. *58*, 8134–8138.

Dean, J.A., and Lange, N.A. (1999). Lange's Handbook of Chemistry, Fifteenth Edition (McGraw-Hill).

Decrey, L., Bonvin, F., Bonvin, C., Bonvin, E., and Kohn, T. (2020). Removal of trace organic contaminants from wastewater by superfine powdered activated carbon (SPAC) is neither affected by SPAC dispersal nor coagulation. Water Res. *185*, 116302.

Ding, Q., Yamamura, H., Yonekawa, H., Aoki, N., Murata, N., Hafuka, A., and Watanabe, Y. (2018). Differences in behaviour of three biopolymer constituents in coagulation with polyaluminium

chloride: implications for the optimisation of a coagulation-membrane filtration process. Water Res. *133*, 255–263.

Du, H., Yang, Z., Tian, Z., Huang, M., Yang, W., Zhang, L., and Li, A. (2018). Enhanced removal of trace antibiotics from turbid water in the coexistence of natural organic matters using phenylalanine-modified-chitosan flocculants: effect of flocculants' molecular architectures. Chem. Eng. J. *333*, 310–319.

Frisch, M.J., Trucks, G.W., Schlegel, H.B., Scuseria, G.E., Robb, M.A., Cheeseman, J.R., Scalmani, G., Barone, V., Mennucci, B., Petersson, G.A., et al. (2009). Gaussian 09, Revision E.01 (Gaussian Inc).

Grandclement, C., Seyssiecq, I., Piram, A., Wong-Wah-Chung, P., Vanot, G., Tiliacos, N., Roche, N.,

and Doumenq, P. (2017). From the conventional biological wastewater treatment to hybrid processes, the evaluation of organic micropollutant removal: a review. Water Res. *111*, 297–317.

Gu, J., Fan, H., Li, C., Caro, J., and Meng, H. (2019). Robust superhydrophobic/superoleophilic wrinkled microspherical MOF@rGO composites for efficient oil-water separation. Angew. Chem. Int. Ed. *58*, 5297–5301.

Hamley, I.W. (2003). Nanotechnology with soft materials. Angew. Chem. Int. Ed. *2003*, 1692–1712.

Herrmann, S., De Matteis, L., de la Fuente, J.M., Mitchell, S.G., and Streb, C. (2017). Removal of multiple contaminants from water by polyoxometalate supported ionic liquid phases (POM-SILPs). Angew. Chem. Int. Ed. *56*, 1667–1670.

Holmberg, K., Jonsson, B., Kronberg, B., and Lindman, B. (2002). Surfactants and Polymers in Aqueous Solution (John Wiley & Sons, Ltd.).

Jiang, M., Eisenberg, A., Liu, G.J., and Zhang, X. (2006). Macromolecular Self-Assembly (Science Press).

Larsen, T.A., Hoffmann, S., Luthi, C., Truffer, B., and Maurer, M. (2016). Emerging solutions to the water challenges of an urbanizing world. Science *352*, 928–933.

Liu, J., Cheng, S., Cao, N., Geng, C., He, C., Shi, Q., Xu, C., Ni, J., DuChanois, R.M., Elimelech, M., and Zhao, H. (2019). Actinia-like multifunctional nanocoagulant for single-step removal of water contaminants. Nat. Nanotechnol. *14*, 64.

Miller, D.J., Dreyer, D.R., Bielawski, C.W., Paul, D.R., and Freeman, B.D. (2017). Surface modification of water purification membranes. Angew. Chem. Int. Ed. *56*, 4662–4711.

Qin, X.F., Yu, C.M., Wei, J., Li, L., Zhang, C.W., Wu, Q., Liu, J.H., Yao, S.Q., and Huang, W. (2019). Rational design of nanocarriers for intracellular protein delivery. Adv. Mat. *31*, 1902791.

Ren, K., Du, H., Yang, Z., Tian, Z., Zhang, X., Yang, W., and Chen, J. (2017). Separation and sequential recovery of tetracycline and Cu(II) from water using reusable thermoresponsive chitosan-based flocculant. ACS Appl. Mater. Inter. *9*, 10266–10275.

Richardson, S.D., and Kimura, S.Y. (2020). Water analysis: emerging contaminants and current issues. Anal. Chem. *92*, 473–505.

Schwarzenbach, R., Escher, B., Fenner, K., Hofstetter, T., Johnson, C., Von Gunten, U., and Wehrli, B. (2006). The challenge of micropollutants in aquatic systems. Science *313*, 1072–1077.

Shannon, M., Bohn, P., Elimelech, M., Georgiadis, J., Mariñas, B., and Mayes, A. (2008). Science and technology for water purification in the coming decades. Nature *452*, 301–310.

Simate, G.S., Iyuke, S.E., Ndlovu, S., and Heydenrych, M. (2012). The heterogeneous coagulation and flocculation of brewery wastewater using carbon nanotubes. Water Re *46* (4), 1185–1197.

Sun, H. (1998a). COMPASS: an ab initio force-field optimized for condensed-phase applications overview with details on alkane and benzene compounds. J. Phys. Chem. B *102* (38), 7338–7364.

Sun, H., Ren, P., and Fried, J.R. (1998b). The COMPASS force field: parameterization and validation for phosphazenes. Comput. Theor. Polym. Sci. *8* (1), 229–246.

Sun, T.M., Zhang, Y.S., Pang, B., Hyun, D.C., Yang, M.X., and Xia, Y.N. (2014). Engineered nanoparticles for drug delivery in cancer therapy. Angew. Chem. Int. Ed. *53* (46), 12320–12364.

United Nations (2021). Ensure Availability and Sustainable Management of Water and Sanitation for All. https://sdgs.un.org/goals/goal6.

Wang, J., Shen, H., Hu, X., Li, Y., Li, Z., Xu, J., Song, X., Zeng, H., and Yuan, Q. (2016). A targeted "capture" and "removal" scavenger toward multiple pollutants for water remediation based on molecular recognition. Adv. Sci. *3*, 1500289.

Wang, X., Wang, X., Wei, Z., and Zhang, S. (2018). Potent removal of cyanobacteria with controlled release of toxic secondary metabolites by a titanium xerogel coagulant. Water Res. *128*, 341–349.

Wang, Y., Hou, T., Yang, Z., Zhao, L., Wu, W., Yang, W., and Graham, N.J.D. (2020a). Nitrogen-free cationic starch flocculants: flocculation performance, antibacterial ability, and uf membrane fouling control. ACS Appl. Bio Mater. *3*, 2910–2919.

Wang, Y., Pan, T., Yu, Y., Wu, Y., Pan, Y., and Yang, X. (2020b). A novel peroxymonosulfate (PMS)-enhanced iron coagulation process for simultaneous removal of trace organic pollutants in water. Water Res. *185*, 116136.

Wu, B.R., Dai, X.H., and Chai, X.L. (2020). Critical review on dewatering of sewage sludge: Influential mechanism, conditioning technologies and implications to sludge re-utilizations. Water Res. *180*, 115912.

Yang, Z., Degorce-Dumas, J.-R., Yang, H., Guibal, E., Li, A., and Cheng, R. (2014a). Flocculation of Escherichia coli using a quaternary ammonium salt grafted carboxymethyl chitosan flocculant. Environ. Sci. Technol. *48*, 6867–6873.

Yang, Z., Hou, T., Ma, J., Yuan, B., Tian, Z., Yang, W., and Graham, N.J.D. (2020). Role of moderately hydrophobic chitosan flocculants in the removal of trace antibiotics from water and membrane fouling control. Water Res. *177*, 115775.

Yang, Z., Li, H.J., Yan, H., Wu, H., Yang, H., Wu, Q., Li, H.B., Li, A.M., and Cheng, R.S. (2014b). Evaluation of a novel chitosan-based flocculant with high flocculation performance, low toxicity and good floc properties. J. Hazard. Mater. *276*, 480–488.

Yang, Z., Ren, K., Guibal, E., Jia, S., Shen, J., Zhang, X., and Yang, W. (2016). Removal of trace nonylphenol from water in the coexistence of suspended inorganic particles and NOMs by using a cellulose-based flocculant. Chemosphere *161*, 482–490.

Yang, Z., Yan, H., Yang, H., Li, H.B., Li, A.M., and Cheng, R.S. (2013). Flocculation performance and mechanism of graphene oxide for removal of various contaminants from water. Water Res. *47*, 3037–3046.

Yu, J., Li, G., Liu, H., Zeng, L., Zhao, L., Jia, J., Zhang, M., Zhou, W., Liu, H., and Hu, Y. (2019). Electrochemical flocculation integrated hydrogen evolution reaction of Fe@N-Doped carbon nanotubes on iron foam for ultralow voltage electrolysis in neutral media. Adv. Sci. *6*, 1901458.

Zhang, Q.R., Bolisetty, S., Cao, Y.P., Handschin, S., Adamcik, J., Peng, Q.M., and Mezzenga, R. (2019a). Selective and efficient removal of fluoride from water: in situ engineered amyloid fibril/ZrO2 hybrid membranes. Angew. Chem. Int. Ed. *58*, 6012–6016.

Zhang, T., Lowry, G.V., Capiro, N.L., Chen, J.M., Chen, W., Chen, Y.S., Dionysiou, D.D., Elliott, D.W., Ghoshal, S., Hofmann, T., et al. (2019b). In situ remediation of subsurface contamination: opportunities and challenges for nanotechnology and advanced materials. Environ. Sci. Nano *6*, 1283–1302.

STAR★METHODS

KEY RESOURCES TABLE

REAGENT or RESOURCE	SOURCE	IDENTIFIER
Chemicals, peptides, and recombinant proteins		
3-(trimethoxysilyl)propyl-n-octadecyldimethylammonium chloride	Sigma-Aldrich, Inc.	Cat#595888
$AlCl_3$	Sinopharm Group Co., Ltd.	Cat#20000818
$FeCl_3$	Sinopharm Group Co., Ltd.	Cat#10011918
$TiCl_4$	Sinopharm Group Co., Ltd.	Cat#80130560
Norfloxacin	Dalian Meilun Biotechnology Co. Ltd.	Cat#MB1351
Sulfamethoxazole	Dalian Meilun Biotechnology Co. Ltd.	Cat#MB1320
Tylosin	Dalian Meilun Biotechnology Co. Ltd.	Cat#MB5101
Diclofenac	Dalian Meilun Biotechnology Co. Ltd.	Cat#MB1277
Experimental models: organisms/strains		
Daphnia magna	National Institue of Environmental Health, CDC, China	62 Dm pure strain
Software and algorithms		
Gaussian 09	Frisch et al., 2009; Gaussian, Inc.	https://gaussian.com
Materials Studio 2019	Accelrys Software, Inc.	https://accelrys.com
Other		
IR spectrometer (Bruker IFS 66/S)	Bruker Co.	https://bruker.com
TEM (JOEL JEM-2100F)	JEOL Ltd.	https://jeol.co.jp/
Zetasizer (Malvern Nano-Z)	Malvern Panalytical Ltd.	https://malvernpanalytical.com/en/
Telescopic goniometer (Rame-Hart-100)	Ramé-hart Instrument Co.	https://ramehart.com
Fluorescence microscope (Nikon CFI60)	Nikon Co.	https://nikon.com/
SEM (JEOL JSM-5610LV)	JEOL Ltd.	https://jeol.co.jp/
XPS spectrometer (Thermo Fisher Scientific ESCALAB Xi+)	Thermo Fisher Scientific Inc.	https://thermofisher.com
GC (Agilent 8890)	Agilent Technologies, Inc.	https://agilent.com
MS (Agilent 5977B)	Agilent Technologies, Inc.	https://agilent.com
Turbidimeter (Shanghai Xinrui WGZ-200)	Shanghai Xinrui Instrument Co., Ltd	https://shxr17.com/
UV-vis spectrophotometer (Hitachi UH5300)	Hitachi, Ltd.	https://hitachi.com
TOC analyzer (OI 1030D)	O.I. Co.	https://oico.com
Chemical analyzer (CleverChem 380)	DeChem-Tech. GmbH	https://dechem-tech.de
UPLC-ESI-MS (Thermo Finnigan TSQ Quantum)	Thermo Fisher Scientific Inc.	https://thermofisher.com
CST equipment (Triton 304M)	Triton Electronics Ltd.	https://tritonel.com
ICP emission spectrometer (PerkinElmer Avio 500)	PerkinElmer Inc.	https://perkinelmer.com

RESOURCE AVAILABILITY

Lead contact

Further information and requests for resources and reagents should be directed to and will be fulfilled by the lead contact, Dr. Zhen Yang (yangzhen@njnu.edu.cn).

Materials availability

The newly generated hydrophobic-organic-chain-modified metal hydroxide flocculants in this manuscript, involving HOC-Al, HOC-Fe, and HOC-Ti, will be made available on request, but we may require a payment and/or a completed Materials Transfer Agreement if there is potential for commercial application.

Data and code availability

This study did not generate any dataset/code.

EXPERIMENTAL MODEL AND SUBJECT DETAILS

The tested *Daphnia magna* (a 62 Dm pure strain) for acute toxicity assays were cultured for more than 3 generations and new-born within 6–24 hr under lab conditions. Every 10 *Daphnia magna* were cultured in 500 mL of water with a *Scenedesmus obliquus* (strain number: FACHB-276) concentration of 6×10^6/mL in a 1-L beaker under the indoor natural light conditions at 25°C. pH of the solution was 7.5 ± 0.5 and dissolved oxygen was more than 2 mg/L.

METHOD DETAILS

Synthesis of HOC-M

3-(trimethoxysilyl)propyl-n-octadecyldimethylammonium chloride (DTSACl) was firstly diluted in a solvent mixture of ethanol, water and HCl to produce a volume ratio of 100:3000:1:1000 for DTSACl:ethanol:HCl:water. After mechanically stirring for 24 hr at 25°C, the mixture was then dialyzed for 12 hr using a dilute HCl solution (pH = 2.2) as the dialysate (replaced every 2 hr) and a dialysis membrane (molecular weight cut-off of 100 Da), to separate hydrolyzed DTSACl from ethanol. The hydrolyzed DTSACl was then added into MCl_n ($AlCl_3$, $FeCl_3$ or $TiCl_4$) aqueous solution to reach a target ratio of octadecyl: metal atom (1:5, 1:10, or 1:15). Reaction took place under mechanical stirring at 25°C for 12 hr after the pH of the mixture was adjusted to a pre-optimized value (3.5, 4.0 and 1.5 for HOC-Al, HOC-Fe and HOC-Ti, respectively) by dilute NaOH (1 mol/L). After the total metal concentration was adjusted to 0.1 mol/L, the resulting solution was allowed to stand for another 12 hr of aging at 25°C, which completed the preparation of the self-assembled micelle-like nanoparticles. Unit prices of raw materials and the calculated prices of HOC-M10 were listed in Table S4.

Flocculation tests

Raw surface water (water quality parameters listed in Table S2) was freshly collected from the Ma'anshan section of Yangtze River (raw water collection site at Caishi Water Factory, Ma'anshan, Anhui Province; 31°38′49″N 118°27′06″E) and stored at 4°C. Before the flocculation tests, model pharmaceuticals (norfloxacin (NOR), sulfamethoxazole (SMXL), tylosin (TYL) and diclofenac (DCF)), with basic information in Table S3, were manually added into real surface water to obtain an equilibrium concentration of 100 ng/L for each pharmaceutical in water at 25°C.

Static jar flocculation tests were conducted using a programmable flocculator (Figure 2A; Wuhan Meiyu MY3000-6B) at 25°C. After a known volume of the flocculant stock solution was dosed, the flocculation procedure included three steps as follows: 5 min of rapid mixing for full contact between the flocculants and contaminants at 200 rpm, 15 min of slow mixing for large floc growth at 50 rpm, and finally 30 min of floc settling. Here, 30 min of floc settling was enough since turbidities of surpernatant water samples under most conditions were stable in this work. After settling, samples of the supernatant water and flocs were carefully collected for further analysis.

Continuous-flow flocculation tests were conducted using a custom-made apparatus (Figures 2B and 2C; a simplified and reduced-scale model of real facilities at WTWs). The water flow rate of the apparatus was 0.5 L/hr. Both raw water and flocculant stock solution were pumped with pre-designated flow rates into the first flocculation tank. The optimal dosages of different flocculants were obtained from the jar tests. The stirring speeds of the four flocculation tanks were 200, 150, 100, and 50 rpm, respectively, for floc growth. Then, water containing visible large flocs flowed into an inclined plate settling tank for floc sedimentation. The hydraulic residence time (HRT) of each flocculation tank and the settling tank was 5 min and 1 hr, respectively. The produced water was collected every 30 min for water quality determination. After each test was run for 6 hr, flocs in the settling tank were carefully collected for further analysis.

Floc dewatering tests were conducted using a mechanical pressure filter device. The dewatering procedures included three steps as follows: 400 kPa for 15 min, 600 kPa for 50 min, and 900 kPa for 30 min.

Characterizations and analyses

Fourier transform infrared spectra were recorded using an infrared spectrometer (Bruker IFS 66/S). Transmission electron microscope (TEM) images were obtained using a TEM (JOEL JEM-2100F) at an acceleration voltage of 200 kV. Energy dispersive X-ray (EDX) mapping images were obtained using an EDX spectroscopy attached with the TEM. Zeta potentials and size distributions were measured using a Zetasizer (Malvern Nano-Z). Water contact angles were determined using a telescopic goniometer (Rame-Hart-100). Fluorescence images were obtained using a fluorescence microscope (Nikon CFI60). Scanning electron microscopy (SEM) images were obtained using an SEM (JEOL JSM-5610LV). X-ray photoelectron spectra (XPS) were recorded by an XPS spectrometer (Thermo Fisher Scientific ESCALAB Xi+). Acute toxicity assays of the flocculants were carried out using newborn (<24 hr) *Daphnia magna* to determine the 24 hr-halfmaximal effective concentration (24hr-EC50). N-containing disinfection by-product (N-DBP) detection of the flocculants were conducted as follows: firstly, monochloramine solution (2 mmol/L; in phosphate buffer saline) was prepared using sodium hypochlorite and ammonium chloride with a Cl_2:N ratio of 4.75:1; then, a certain type of flocculant was added to a concentration of 10 mg/L; the solution was incubated for 10 days in the dark at 20°C before ascorbic acid with two times effective concentration was added to stop the reaction; finally, samples after solid phase extraction, elution, and nitrogen blow down evaporation were detected using a gas chromatograph (Agilent 8890) coupled with a quadrupole mass spectrometer (Agilent 5977B) with an inert ion source. Information about reference N-DBPs in GC-MS were listed in Table S1.

Turbidity was measured using a turbidimeter (Shanghai Xinrui WGZ-200). UV_{254} absorbance of water (after filtration by a 450-nm membrane) was determined using a UV-vis spectrophotometer (Hitachi UH5300). Dissolved organic carbon (DOC) of water (after filtration by a 450-nm membrane) was determined using a total organic carbon analyzer (OI 1030D). NO_3^--N and total phosphate were measured using a chemical analyzer (CleverChem 380). Pharmaceutical concentrations after solid phase extraction (SPE) were determined using an ultra-performance liquid chromatograph coupled to an electrospray ionization mass spectrometer (UPLC-ESI-MS; Thermo Finnigan TSQ Quantum), with a Sepax C18 column (2.1 × 100 mm, 5 μm). Floc size (characteristic length, L) and two-dimensional fractal dimension (D_2, defined by the power law relationship between projected area A and L) were determined using an image analysis method. Here, L was defined as the largest projection length. A and L were derived from floc photos (captured by an optical microscope) using Image-pro Plus 6.0. The value of D_2 was then obtained from the slope of the log-log plot of A and L (Figures S16 and S17). Specific filtration resistance (SFR) was measured using the vacuum filtration method, in which a standard Büchner funnel was used and the pressure was 0.07 MPa. Capillary suction time (CST) was measured using a CST equipment (Triton 304M). The water content of flocs after dewatering was calculated from sample weight loss at 105°C. Metal ion concentrations in the treated water were determined by an inductively coupled plasma (ICP) emission spectrometer (PerkinElmer Avio 500).

Theoretical chemical computations

Molecular dynamics (MD) simulation, in which 16 HOC-M chains were simulated with 500 H_2O molecules in a 7 nm × 7 nm × 7 nm cube, was performed using modules of Materials Visualizer, Amorphous Cell, and Forcite in Materials Studio software. Calculations were based on Compass II Forcefield (CVFF) for 1 ns using NPT system and followed by 2 ns using NVT system (Sun 1998a; Sun et al., 1998b). Density functional theory (DFT) computations of optimized spatial configurations of typical fragments of flocculants and contaminants, as well as pairwise complexes, were performed using the Gaussian 09 software at the M06e2x/6–31 + G(d) level. BE was calculated according to the equation (BE = $|E_{flocculant-contaminant} - E_{flocculant} - E_{contaminant}|$, where $E_{flocculant-contaminant}$, $E_{flocculant}$, and $E_{contaminant}$ were energies of the optimized geometry of a complex, the fragment of the flocculant, and the contaminant, respectively (Frisch et al., 2009).

QUANTIFICATION AND STATISTICAL ANALYSIS

Information about statistics have been given in the figure titles of Figures 1, 2, S5, S8–S11, and S18.